HHS Public Access

Author manuscript

Neurobiol Dis. Author manuscript; available in PMC 2021 August 18.

Published in final edited form as:

Neurobiol Dis. 2021 May ; 152: 105277. doi:10.1016/j.nbd.2021.105277.

Mutant three-repeat tau expression initiates retinal ganglion cell death through Caspase-2

Jennifer Ngolab[a], **Saranya Canchi**[a,c], **Suhail Rasool**[a,d], **Abderrahman Elmaarouf**[b], **Kimberly Thomas**[b], **Floyd Sarsoza**[a,c], **Jennifer Grundman**[a], **Michael Mante**[a], **Jazmin Florio**[a], **Nimisha Nandankar**[a], **Shaina Korouri**[a], **Wagner Zago**[b], **Eliezer Masliah**[e], **Robert A. Rissman**[a,c,*]

[a]Department of Neurosciences, University of California, San Diego, School of Medicine, La Jolla, CA 92093, United States of America

[b]Prothena Biosciences, South San Francisco, CA 94080, United States of America

[c]Veterans Affairs San Diego Healthcare System, San Diego, CA 92161, United States of America

[d]Amydis Inc, San Diego, CA 92121, United States of America

[e]Division of Neuroscience and Laboratory of Neurogenetics, National Institutes on Aging, NIH, Bethesda, MD 20892, United States of America

Abstract

The microtubule-associated protein tau is implicated in multiple degenerative diseases including retinal diseases such as glaucoma; however, the way tau initiates retinopathy is unclear. Previous retinal assessments in mouse models of tauopathy suggest that mutations in four-repeat (4R) tau are associated with disease-induced retinal dysfunction, while shifting tau isoform ratio to favor three-repeat (3R) tau production enhanced photoreceptor function. To further understand how alterations in tau expression impact the retina, we analyzed the retinas of transgenic mice overexpressing mutant 3R tau (m3R tau-Tg), a model known to exhibit Pick's Disease pathology in the brain. Analysis of retinal cross-sections from young (3 month) and adult (9 month) mice detected asymmetric 3R tau immunoreactivity in m3R tau-Tg retina, concentrated in the retinal ganglion and amacrine cells of the dorsal retinal periphery. Accumulation of hyperphosphorylated tau was detected specifically in the detergent insoluble fraction of the adult m3R tau-Tg retina. RNA-seq analysis highlighted biological pathways associated with tauopathy that were uniquely

*Corresponding author at: Department of Neurosciences, UCSD School of Medicine, 9500 Gilman Drive, MTF 309, M/C 0624, La Jolla, CA 92093-0624, United States of America, rrissman@health.ucsd.edu (R.A. Rissman).

CRediT authorship contribution statement

Jennifer Ngolab: Conceptualization, Methodology, Investigation, Writing - original draft, Writing - review & editing, Supervision, Visualization. **Saranya Canchi**: Conceptualization, Methodology, Software, Formal analysis, Writing - review & editing, Visualization. Suhail Rasool: Methodology, Investigation, Writing - review & editing. **Abderrahman Elmaarouf**: Conceptualization, Methodology, Investigation, Writing - review & editing, Resources, Supervision, Formal analysis. **Kimberly Thomas**: Investigation, Resources. **Floyd Sarsoza**: Investigation, Visualization. **Jennifer Grundman**: Investigation, Writing - review & editing. **Michael Mante**: Investigation, Formal analysis. **Jazmin Florio**: Investigation. **Nimisha Nandankar**: Investigation. **Shaina Kokouri**: Investigation, review and editing. **Wagner Zago**: Conceptualization, Resources, Supervision. **Eliezer Masliah**: Conceptualization, Writing - review & editing, Supervision. **Robert A. Rissman**: Conceptualization, Methodology, Writing - review & editing, Supervision, Funding acquisition.

Appendix A. Supplementary data

Supplementary data to this article can be found online at https://doi.org/10.1016/j.nbd.2021.105277.

altered in m3R tau-Tg retina. The upregulation of transcript encoding apoptotic protease caspase-2 coincided with increased immunostaining in predominantly 3R tau positive retinal regions. In adult m3R tau-Tg, the dorsal peripheral retina of the adult m3R tau-Tg exhibited decreased cell density in the ganglion cell layer (GCL) and reduced thickness of the inner plexiform layer (IPL) compared to the ventral peripheral retina. Together, these data indicate that mutant 3R tau may mediate toxicity in retinal ganglion cells (RGC) by promoting caspase-2 expression which results in RGC degeneration. The m3R tau-Tg line has the potential to be used to assess tau-mediated RGC degeneration and test novel therapeutics for degenerative diseases such as glaucoma.

Keywords

Retina; Tau; 3 repeat tau; Retinopathy; Alzheimer's, tauopathy

1. Introduction

The microtubule-associated protein tau is a scaffolding protein implicated in the pathophysiology of neurodegenerative diseases related to dementia (Josephs, 2017). Alternative splicing of the *MAPT* gene produces distinct tau isoforms, differing in the number of microtubule-binding repeats and amino-terminal inserts (Goedert et al., 1989). Modifications to tau, including single nucleotide polymorphisms within MAPT and hyperphosphorylation, mediate neurofibrillary tangle formation and ultimately lead to neurodegeneration (Arendt et al., 2016; Wang and Mandelkow, 2016). Tauopathies are neurodegenerative disorders characterized by abnormal cerebral tau aggregates and broadly categorized by tau isoform (Josephs, 2017; Kovacs, 2015). Neurofibrillary tangles comprised of four-repeat (4R) tau are found in patients diagnosed with progressive supranuclear palsy, while three-repeat (3R) intracellular inclusions are a characteristic of Pick's Disease (Goedert et al., 2018). Mutations in MAPT, such as the familial Pick's Disease mutation L266V, are associated with a shift in tau isoform ratio (Hogg et al., 2003).

Hyperphosphorylated tau in the retina is observed in other neurodegenerative diseases such as glaucoma and Alzheimer's Disease (AD) (den Haan et al., 2018; Gupta et al., 2008). The retina is a multilayered neural tissue optimized to convert light into neuronal signals (Masland, 2012) through stimulation of the photoreceptors. The inner plexiform layer (IPL) refines additional visual features through a synaptic network between retinal subpopulations, including spatial-temporal information computed by amacrine cells (Diamond, 2017). The final retinal visual output is transmitted to the brain via the retinal ganglion cells (RGCs). Visual impairment often manifests due to retinal perturbations such as retinal cell death (Hoon et al., 2014). Retinal cell loss is mediated by the cysteine aspartate protease family known as caspases in cases of ocular injury (Thomas et al., 2017). Tau is cleaved by executioner caspases in early state AD, preceding tau hyperphosphorylation (Rissman et al., 2004), however the mechanisms of retinal tau pathology are unclear. Retinal thinning and photoreceptor dysfunction were observed in transgenic mouse models expressing mutant hyperphosphorylated tau (Gasparini et al., 2011; Harrison et al., 2019; Ho et al., 2015; Mazzaro et al., 2016). However, photoreceptor performance was enhanced in a mouse model

expressing human tau (Rodriguez et al., 2018), suggesting that the mutations on tau, rather than isoform imbalance, may mediate retinal dysfunction.

Genomic studies have provided insight into the molecular underpinnings of retinopathy such as the localization of genetic variants associated with Age-related macular degeneration to 20 specific chromosomal loci (Fritsche et al., 2014). With the advent of next-generation sequencing, additional information has been gleaned from disease models, as the depth of coverage along with the large amount of data produced by transcriptomic profiling provide a comprehensive global snapshot of a tissue. Studies of the retina through whole-exome and single-cell RNA-sequencing highlighted alterations in retinal transcript expression with age and disease (Menon et al., 2019; Voigt et al., 2019). Next-generation sequencing technology may provide insight into understanding the implications of mutant tau in the retina.

To fully understand the extent of tau pathology on the retina, we characterized the retinas of mice overexpressing mutant 3R tau (m3R tau-Tg) shown to confer Pick's Disease pathology (Arner et al., 2018; Rockenstein et al., 2015). Since the promoter driving mutant 3R tau expression in this strain is the RGC marker Thy-1, (Schmid et al., 1995) we hypothesized that mutant 3R tau would exhibit visual impairment due to tau-mediated RGC neurodegeneration. To test this hypothesis, we applied a comprehensive analysis including behavioral, immunohistochemical and molecular techniques to characterize the m3R tau-Tg retina. Retinal mutant 3R tau was restricted to the dorsal periphery, where it was associated with structural alterations. Overexpression of 3R tau in the retina over time led to the differential expression of genes implicated in neurodegeneration, including caspase-2. Increased expression of caspase-2 in m3R tau-Tg retinas coincided with reduction of RGCs. In summary, we have demonstrated that mutant 3R tau may alter retinal structure through RGC degeneration via apoptotic pathways. These structural changes may alter performance in behaviors that rely on vision.

2. Materials and methods

2.1. Animals

All rodent experiments complied with NIH guidelines for good animal care and use, and all procedures were reviewed and approved by the University of California San Diego Institutional Animal Care and Use Committee. Male and female transgenic mice from Line 13, a line expressing high levels of human 3R tau with the L266V and G272V mutations associated with familial Pick's Disease and driven by the neuronal mThy-1 promoter, (m3R tau-Tg) along with non-transgenic littermates (Non-Tg) were used in all experiments (Rockenstein et al., 2015). The m3R tau-Tg line has been previously characterized, exhibiting behavioral and pathological characteristics of Pick's Disease (Arner et al., 2018; Rockenstein et al., 2015). Mice were maintained on a standard 12 h on/off light cycle; water and food were provided ad libitum.

2.2. Western blot

Mouse retinas and brains from 9 month old m3Rtau-Tg and Non-tg mice were homogenized to yield a detergent soluble as well as insoluble cellular fraction. For the retinal samples,

6 mouse retinas were pooled and then lysed using 2 μl/mg detergent free RAB buffer containing 100 mM 2-(N-morpholino) ethanesulphonic acid (MES; pH 7.0), 1 mM EGTA, 0.5 mM $MgSO_4$, 750 mM NaCl, 20 mM NaF, 1 mM Na_3VO_4, 1 mM PMSF, and EDTA-free protease and phosphatase inhibitor cocktail (Thermo Scientific). Brain sections containing hippocampus and cortex were similarly prepared. Chilled samples were homogenized then centrifuged at 40,000 ×*g* for 30 min at 4 °C. The supernatant from each sample was collected, and the remaining pellet was resuspended in RAB buffer on ice. After centrifugation at 40,000 ×*g* for 30 min at 4 °C, the supernatants containing RAB-soluble proteins were collected and pooled with the supernatants collected during the previous spin. To collect detergent-soluble proteins, pellets from each sample were resuspended in 2 μl/mg RIPA buffer containing 50 mM Tris (pH 7.4), 1 mM EDTA, 1 mM EGTA, 150 mM NaCl, 10 mM NaF, 1 mM Na_3VO_4, 1 μM okadaic acid, 1% NP40, 1% Triton X-100, 0.25% sodium deoxycholate, 0.1% SDS, 1 mM PMSF and protease inhibitor. Samples were centrifuged at 40,000 ×*g* for 30 min at 4 °C, and the supernatant was collected. Protein concentrations were determined using a BCA Protein Assay Kit. Proteins were then boiled in sample buffer containing SDS, 2-mercaptoethanol, and glycerol at 95 °C for 5 min.

Western blot analysis was performed on RAB and RIPA fractions to assess tau expression in the retina. 15 μg of protein from retina and 2 μg from brain were loaded and electrophoretically separated on a 10–20% Tris-HCL criterion gel (Bio-Rad, Hercules, CA). Proteins were transferred to a 0.45 μm PVDF membrane, blocked in 5% BSA-TBS-Tween for 30 min at room temperature, and then incubated in primary antibodies diluted in 5% TBS-Tween overnight at 4 °C. Primary antibodies were detected using horseradish peroxidase-linked (HRP) secondary antibodies and developed with an enhanced chemiluminescence Western blot detection kit (Supersignal West Pico, Pierce Biotechnology). Gel images were obtained using a BioRad ChemiDoc XRS, and quantitative band intensity readings were made using the accompanying BioRad Image software. To characterize retinal tau expression, we utilized two well-characterized antibodies: RD3 (1:1000) to detect 3R tau and PHF-1 (1:1000) to detect phosphorylated tau. Semi-quantitative measurement of immunoblots were conducted through densitometry. Complete blots can be found in the Supplementary Data section.

2.3. Behavioral studies

A large cohort of m3R tau-Tg and Non-Tg mice underwent behavioral analysis. A total of 12 Non-Tg (male: 6, female: 6) and 15 m3R tau-Tg (male: 7, female: 8) aged at 3 months were tested for motor, visual and cognitive deficits. A total of 15 Non-Tg (male: 3, female: 12) and 26 m3R tau-Tg (male: 12, female:14). To determine visual spatial ability and memory retention over time, mice underwent assessment in the Morris Water Maze as previously described (Arner et al., 2018; Rockenstein et al., 2015). Briefly, mice were placed in a 180 cm diameter pool filled with opaque water at 24 °C and tasked to swim to a platform. Entry into the pool for each mouse was randomly selected between two entry points equidistant from the platform. Throughout the test, the platform was placed in the same quadrant. The test consisted of two phases: the Cued Platform and the Hidden Platform phase. Days 1 to 3 are the Cued Platform Phase, where the platform remained visible to train the mouse to swim to the platform. For the Hidden Platform Phase, the platform

was submerged on day 4 and mice underwent three consecutive trials separated 2–3 min apart each day for 4 days. Mice that did not locate the hidden platform within 90 s were brought to the platform and placed on top for 30 s. Two additional tests were performed on the final trial day to assess memory retention (Probe test) and visual acuity (Visual Probe test). In the Probe test, mice were placed into the pool without a platform for 40 s and the number of times the mouse entered the quadrant where the platform was located was tabulated. The Visual Probe test measured the amount of time a mouse spent swimming to a visible platform. Time spent swimming to the platform, distance travelled, and number of entries into the correct quadrant were recorded using the AnyMaze video tracking software (Stoelting Co, Wood Dale, IL, USA) set to analyze two samples per second.

Overall locomotor activity was measured in a high-density cage placed into a Kinder Smart Frame cage rack system (Kinder Scientific, Poway, CA). The system emits photobeams across the cage floor in a 7 × 15 beam configuration, allowing for the continuous monitoring of the animal's location in X, Y, Z coordinate space. Data acquisition begins once an individual animal is placed into the test chamber, and the test session duration lasted 10 min per mouse.

2.4. Immunohistological staining of mouse eye cross-sections

Postmortem mouse eyes were enucleated and stored in *Z*-Fixative (Excalibur Pathology, Norman, OK) at room temperature, then embedded in paraffin. Eye globes were sectioned at 10 μm and mounted on charged microslides. Retinal sections used for morphometry were processed using a Leica Bond Rx stainer (Leica Biosystems), in the presence of 3R tau antibody, 1 μg/ml, (1 h at room temperature) then an anti-mouse polymer (Leica Biosystems), with DAB (DAKO) visualization and hematoxylin counterstaining. The slides were imaged in a Nanozoomer digital slide scanner (Hamamatu, Japan). Representative images were post-processed in Adobe Photoshop CC 2020.

2.5. Fluorescent staining of mouse retinal tissue

Both mouse wholemount retinal tissue and eye cross-sections were assessed in our colocalization studies. Paraffinized mouse eye cross-sections mounted on charged microslides were deparaffinized with Citrisolv (Decon Labs, King of Prussia, PA) and treated with 10 mM sodium citrate. Retinal cross-sections were incubated with 0.1% Triton-X and 1% H_2O_2 for 20 min and blocked with 2% normal goat serum for 1 h. The cross-sections were then incubated with primary antibody overnight at 4 °C.

For retinal wholemount assessment, postmortem mouse eyes were enucleated and stored in RNAlater prior to dissection. The anterior segment was excised, and the resulting posterior cup was placed in 4% paraformaldehyde for 20 min at room temperature. The retina was separated from the retinal pigmented epithelium (RPE) and washed three times with 1× PBS for 5 min. Wholemount retinal tissues were incubated with PBS solution with 0.2% Triton-X (PBST) for 20 min and blocked with 2% normal goat serum in PBST for 1 h. After blocking, tissues were incubated in primary antibodies diluted in PBST overnight in 4C.

The following primary antibodies were used in this study: 3R tau (MiliporeSigma, RD3, clone 8E6/C11, 1:300), ChAT (MiliporeSigma, 1:500), TUJ1 (MiliporeSigma, 1:200),

RBPMS (PhosphoSolutions, 1:500) and caspase-2 (Abcam, 1:200). Fluorescent-conjugated secondary antibodies Alexa Fluor 568 and Alexa Fluor 488 were used at 1:1000. All retinal tissues were visualized on a Leica DMI 4000B microscope (Leica, Germany) equipped with a TCS SPE camera and Leica 10, 20 and 40× objectives.

2.6. Retinal quantification

Retinal cross sections were taken at 3.25× magnification and analyzed using ImageJ software. Measurements taken 500 μm from the optic nerve were designated center retinal measurements while measurements taken 500 μm from the edge were labeled as peripheral retinal measurements. A total of 27 cross sections from 3 month mice (m3R tau-Tg $n = 17$, Non-Tg $n = 10$), and 21 cross sections from 9 month mice (m3R tau-Tg $n = 12$, Non-Tg $n = 9$) were measured for retinal thickness. Mean intensity of 3R tau immunostaining in the IPL was measured in the ventral and dorsal retina, along 500 μm beginning at the peripheral tip, using ImageJ. A total of 12 retinal cross sections from 3 month mice (m3R tau-Tg $n = 6$, Non-Tg $n = 6$) and 11 retinal cross sections from 9 month mice (m3R tau-Tg $n = 4$, Non-Tg $n = 7$) were assessed for 3R tau immunostaining intensity. Counts of total RGCs in the retinal ganglion cell layer along the same 500 μm were also determined. A total of 18 cross sections from 3 month mice (m3R tau-Tg $n = 9$, Non-Tg $n = 9$) and 13 cross sections from 9 month mice (m3R tau-Tg $n = 9$, Non-Tg $n = 9$) were quantified for total RGCs.

2.7. Retinal wholemount assessment

The right eyes of both Non-Tg and m3Rtau-Tg mice were marked to designate the nasal region before enucleation. The retina was dissected and notched to signify nasal and temporal regions. Retinal flatmounts were imaged at 20× and analyzed through ImageJ. Peripheral retinal measurements were taken 500 μm from the edge of the retina. Dorsal regions of the retina contained the regions of the retina that were in the superior area, while ventral regions contained segments of the inferior area. Cell counts were taken from three 150 μm^3 measurements from each region. Percent change was calculated to account for sample variation. A total of 8 flatmounts from 9 month mice were analyzed (m3R tau-Tg $n = 4$, Non-Tg $n = 4$).

2.8. Transmission electron microscopy

Mouse retinas stored in RNAlater stabilization solution (Invitrogen, AM7020) were homogenized in 1× RIPA buffer (Cell Signaling) containing protease inhibitor cocktail and PMSF. Formvar-carbon coated copper grid were fixed with 2% PFA and 1% glutaraldehyde for 5 min then incubated in 10 μl of retinal homogenate for 20 min at room temperature. Grids were washed once with 0.01 M PBS and 50 mM glycine for 3 min, then blocked in 1% cold-water fish skin gelatin in PBS for 1 h. The grids were incubated in anti-3RTau antibody cocktail in 1% cold-water fish skin gelatin (1:50, Millipore) for 2 h at room temperature. After washing six times with PBS for 3 min, the grids were transferred to drops of 1% cold-water fish skin gelatin containing anti-mouse gold-conjugated antibodies (1:100, Sigma-Aldrich) and incubated for 1 h. Grids were washed six times with PBS for 3 min, counterstained with 3% (*w*/*v*) uranyl acetate for 5 min, then washed with double distilled water and blotted dry. Protein content was visualized using a JEOL 1200 EX II transmission electron microscope.

2.9. Gene expression analysis

Total RNA was isolated from mouse retinas and stored in RNALater stabilization solution using the RNeasy Plus Mini Kit (Qiagen, #74134). RNA integrity was measured using the Agilent 4200 TapeStation. A RIN number of 7 or above was considered sufficient to proceed with mRNA library preparations. The number of retinas per age per genotype is as follows: 3 month m3R tau-Tg ($n = 5$), 3 month Non-Tg ($n = 4$), 9 month m3R tau-Tg ($n = 5$), 9 month Non-Tg ($n = 5$). The mRNA libraries were generated by the UC San Diego Institute for Genomic Medicine. RNA-seq data (101 bp paired end reads with coverage of 25 million) was obtained from RNA extracted from the mouse retina. Sequencing was performed using an Illumina HiSeq2500 rapid. The quality of the raw FASTQ files were assessed using FASTQC. Adapters and low-quality reads were trimmed using a kmer approach as implemented in BBDuk v38.62. Transcripts were quantified using quasi-mapping mode of Salmon v0.11.3 (Patro et al., 2017) and summarized to gene counts for downstream analysis using the *tximport* v1.10.0 package (Soneson et al., 2015). Genes were retained in the analysis if they achieved counts per million (cpm) > 1 for any retinal sample. Effective library sizes were estimated by TMM scale-normalization prior to analysis to estimate observational weights (Law et al., 2014; Robinson and Oshlack, 2010). For the log-transformed expression data with precision weights, linear regression models were fit to account for the effects of the interaction between age (3 vs 9 month) and genotype (Non-Tg vs m3R tau-Tg). Test for statistical significance was achieved by implementation of a Bayesian strategy of Lönnstedt and Speed as implemented in *R* package *limma* v3.38.3 (Ritchie et al., 2015). Genes are sorted by their posterior error probability (PEP) and considered significant at PEP < 0.05.

To identify the underlying biological functions enriched in m3R tau-Tg and Non-Tg retina, Gene Set Enrichment Analysis (GSEA) was implemented which identifies the enrichment of functionally defined gene sets using a modified Kolmogorov-Smirnov statistic (Subramanian et al., 2005) and the Molecular Signature Database (MSigDb v6.0). Statistical significance after adjusting for multiple testing is defined at FDR < 0.05. Gene set-based permutation test of 1000 permutations was applied. Detailed description of the GSEA algorithm, testing metrics and the implementation have been described previously (Subramanian et al., 2005). Hypergeometric test was utilized to test the statistical significance of the enriched biological process and pathways identified for the unique differential expressed genes for each group (Yu et al., 2012). Overrepresentation enrichment analysis was conducted using the full set of detected genes as the reference gene set, corrected for multiple testing using the Benjamini-Hochberg procedure and a FDR < 0.05 was considered significant. Estimation of the relative abundance of the cell types was achieved using marker gene sets as defined for each of the different cell classes and first principal component of the marker gene expression (Mancarci et al., 2017; Siegert et al., 2012).

2.10. Statistical analysis

All statistical analysis is presented as mean value ± standard error of the mean (SEM). Behavioral data and retinal measurements were tested for normality before statistical analysis. Analysis of variance (ANOVA) followed with Bonferroni multiple-comparisons post hoc analysis was used for all behavioral and retinal measurements. An unpaired

Student's *t*-test analysis was used to analyze differences between transgenic and non-transgenic IPL retinal thickness as well as Western blot quantification. All statistical analysis was performed using GraphPad Prism (Version 7.0d, GraphPad Software, La Jolla, CA).

2.11. Availability of data and materials

The sequences mentioned in this article will be available in the NCBI Sequence Read Archive repository [https://www.ncbi.nlm.nih.gov/sra] under BioSample accession numbers SAMN15642524, SAMN15642525, SAMN15642526, SAMN15642527, SAMN15642528, SAMN15642529, SAMN15642530, SAMN15642531, SAMN15642532, SAMN15642533, SAMN15642534, SAMN15642535, SAMN15642536, SAMN15642537, SAMN15642538, SAMN15642539, SAMN15642540, SAMN15642541 and SAMN15642542.

3. Results

3.1. Expression of 3R tau in retina is localized to the peripheral dorsal region

Paraffinized ocular cross-sections from 3 and 9 month old mice from m3R tau-Tg and Non-Tg were assayed through immunohistochemistry to detect 3R tau expression in the retina. While we found no 3R tau immunoreactivity in 3 month Non-Tg samples (Fig. 1a), there was abundant 3R tau immunoreactivity in 3 month m3R tau-Tg cross-sections. Interestingly, the staining was strongest in the peripheral dorsal region, and gradually decreased in intensity to completely disappear in the peripheral ventral region (Fig. 1c). Dorsal expression of 3R tau occurred specifically in the intracellular space (Fig. 1b inset) of cell bodies within the GCL as well as in the IPL as diffuse staining (Fig. 1b). The staining in axons of RGCs occurs throughout the nerve fiber layer and inside the optic nerve (Fig. 1a).

No 3R tau immunoreactivity was observed in 9 month Non-Tg retina cross sections (Fig. 1d). Peripheral dorsal 3R tau staining pattern and intensity in 9 month m3R tau-Tg cross sections was similar to 3 month samples (Fig. 1f). Again, strong immunoreactivity was observed in RGCs and the IPL, and staining in the optic nerve was abundant (Fig. 1e). Beyond optic structures, intense 3R tau staining was observed in peripheral nerve fibers innervating oculomotor muscles in 9 month m3R tau-Tg cross-section (Fig. 1d). Immunoreactivity for TUJ1, a marker for RGCs, colocalized to 3R tau positive cells in 9 month m3R tau-Tg retinas (Fig. 1g). 3R tau immunostaining also colocalized with ChAT, a marker for starburst amacrine cells, in both the GCL and the inner nuclear layer (INL) (Fig. 1h).

Protein extracts from 9 month 3R tau-Tg and Non-Tg retinas were immunolabeled with 3R tau antibody and assessed by electron microscopy. Non-Tg samples were negative for immunogold staining (Fig. 1i, top). The immunopositive structures in 3R tau-Tg lysates formed aggregates, which indicates their potential pathogenic nature (Fig. 1i, bottom).

3.2. Increased expression of hyperphosphorylated retinal tau in m3R tau-Tg retina

To determine the pathological state of retinal tau, retinal and brain tissue from 9 month Non-Tg and m3R tau-Tg mice were assessed through immunoblot. As previously reported, abundant 3R tau was detected in the brain of m3R tau-Tg mice but not Non-Tg (RAB: Fig.

2a, $p < 0.01$; RIPA: Fig. 2e, $p = 0.1841$) (Rockenstein et al., 2015). Similarly, significant levels of 3R tau immunoreactivity were detected in both RAB (Fig. 2b, $p < 0.05$) and RIPA fractions (Fig. 2f, $p < 0.0005$) of the m3R tau-Tg retina. PHF-1 (Phospho-Ser 396/404) was detected in both soluble (Fig. 2c, $p = 0.0718$) and insoluble fractions of the 3R tau brain (Fig. 2g, $p = 0.2512$). Negligible levels of PHF-1 were detected in the soluble fraction of both m3R tau-Tg and Non-Tg retinas (Fig. 2d, $p = 0.1504$) while significant levels of PHF-1 were detected predominantly in the detergent insoluble fraction of m3R tau-Tg retinas (Fig. 2h, $p < 0.05$), indicating tau aggregation in the m3R tau-Tg retina.

3.3. Prolonged expression of 3R tau induces structural alterations in the peripheral dorsal inner retina

To determine if 3R tau overexpression induced thinning of the retina, we measured retinal layer thickness from 3R tau-Tg and Non-Tg retinal cross sections stained with hematoxylin and eosin (Fig. 3a). Measurements of the ganglion cell layer (GCL), inner plexiform layer (IPL), outer nuclear layer (ONL) and photoreceptor layer (PH) were taken from cross-sections of 3R tau-Tg and Non-Tg eyes at the center and peripheral regions (Fig. 3a). There were no significant differences in either 3R tau-Tg nor Non-Tg at the center of the retina at any retinal layer (Fig. 3b). Two way ANOVA analysis of the data from the peripheral region of 3 month 3R tau-Tg and Non-Tg retinas detected a significant main effect in layers ($F_{(3,338)} = 32.34$, $p < 0.0001$) but not in genotype ($F_{(3,338)} = 2.579$, $p = 0.0536$). There was no significant layer x genotype interaction ($F_{(9,334)} = 1.026$, $p = 0.4183$). Post hoc analysis determined the difference in the PH layer in the ventral regions between Non-Tg and 3R tau-Tg to be statistically significant. In the 9 month peripheral cross-sections, two way ANOVA also detected a significant main effect in layers ($F_{(3,294)} = 247.5$, $p < 0.0001$) but not in genotype ($F_{(3,294)} = 2.179$, $p = 0.0910$), nor a significant layer x genotype interaction ($F_{(9,294)} = 0.7183$, $p = 0.6921$). Bonferroni analysis detected a significant difference in IPL thickness between the dorsal and ventral peripheral regions of 3R tau-Tg retinas (Fig. 3c). Further analysis with *t*-test determined a significant difference in the IPL between Non-Tg and 3R tau-Tg ($p < 0.025$, Fig. 3c). These data imply that the expression of 3R tau may alter different layer thickness over time.

To test if 3R tau expression changes cell distribution in the GCL, total cells were quantified in the dorsal and ventral peripheral parts of retinal cross-sections stained with hematoxylin. Quantification of GCL cells revealed a significant difference between dorsal and ventral regions of the 3R tau-Tg but not Non-Tg retina at both 3 and 9 months of age ($F_{(3, 54)} = 10.49$; $P < 0.0001$) (Fig. 3d). We stained retinal flatmounts with RBPMS, a known retinal ganglion cell marker, to understand if peripheral RGCs are uniquely targeted in m3R tau-Tg retinas. Peripheral dorsal retinal regions from m3R tau-Tg mice contained fewer RBPMS+ cells compared to the ventral regions (Fig. 3e). A significant difference of RBPMS+ cells was detected between Non-Tg retinas and the dorsal region of the m3R tau-Tg retinas ($F_{(3,12)} = 5.197$; $P < 0.0157$) (Fig. 3f).

3.4. Differential expression of genes implicated in general neurodegeneration in m3R tau-Tg mice

To further assess the molecular impact of 3R tau overexpression in the retina, transcriptome profiling was performed on RNA extracted from both m3R tau-Tg and Non-Tg mouse retinas at 3 months and 9 months. To account for variation in gene expression within biological replicates, samples were consolidated by genotype and further analysis was conducted to assess the effect of prolonged mutant 3R tau expression on the retinal transcriptome. A total of 2230 genes were identified in m3R tau-Tg and Non-Tg retina, with 1817 specifically identified in m3R tau-Tg and 413 in Non-Tg (Fig. 4a).

To identify biological pathways altered with 3R tau expression, pathway analysis was performed on the dataset of differentially expressed genes from m3R tau-Tg retina and Non-Tg using the REACTOME pathway database. The top six unique pathways enriched in Non-Tg retina relate to neuron function and receptor signaling (Fig. 4b). Pathways enriched in the m3R tau-Tg retinal data set include Complex I biology, metabolism of RNA, signaling pathways such as NOD1/2 and NF-kB as well as trafficking processes (Fig. 4b). Our data indicates that overexpression of 3R tau over time induces transcriptional changes that are distinct from the aging process, particularly in biological pathway implicated in neurodegeneration.

3.5. Upregulation of caspase-2 in 3R-tau Tg retina suggests initiation of cell degeneration

The enrichment of transcript encoding components of the NOD and NF-kB signaling pathway along with the reduction of RGC in m3R tau-Tg retina lead us to search for differentially expressed genes associated with RGC cell death. Transcript levels of caspase-2, a protease implicated in RGC neurodegeneration, were upregulated in m3R tau-Tg retina relative to non-Tg retina (Table 2). To determine if the upregulation of caspase-2 transcript altered protein expression, immunohistochemical analysis for caspase-2 expression was conducted in Non-Tg and m3R tau-Tg retinal tissue. No caspase-2 immunostaining was detected in Non-Tg retina throughout the retinal layers (Fig. 5a–b), while robust caspase-2 signal was observed in m3R tau-Tg retinas, with a majority of caspase-2 signal colocalizing to 3R tau-positive cells (Fig. 5c). Expression of caspase-2 in m3R tau-Tg was restricted to the inner retina, specifically the GCL (Fig. 5d).

3.6. Mice overexpressing 3R tau exhibit visual deficits in the Morris Water Maze

The m3R tau-Tg line has previously demonstrated behavioral deficits in the Morris Water Maze (MWM), a memory test dependent on visual cues (Arner et al., 2018; Rockenstein et al., 2015). To further discern whether alteration of 3R tau in RGCs over time alters water maze performance, 3 month old (n = 29 (m3R tau-Tg), 16 (Non-Tg)) and 9 month old (n = 25 (m3R tau-Tg), 15 (Non-Tg)) m3R tau-Tg and Non-Tg mice were subjected to the MWM. Two-way ANOVA analysis revealed a significant main effect in days ($F_{(6,258)}$ = 8.709, $p < 0.0001$) and genotype ($F_{(1,43)}$ = 18.83, $p < 0.0001$) but not a significant interaction in genotype x days ($F_{(6,258)}$ = 1.411, $p = 0.2106$) at three months (Fig. 6a). At nine months, two-way ANOVA analysis revealed a significant interaction between genotype x age ($F_{(6,228)}$ = 6.062, $p < 0.0001$) and a significant main effect in genotype ($F_{(1,38)}$ = 18.82, $p < 0.0001$) and age ($F_{(6,228)}$ = 26.4, $p < 0.0001$) (Fig. 6B). A decrease in distance

travelled over trials in the Cued Platform Phase is an indication of the mice acquiring spatial cues to find the platform (Vorhees and Williams, 2006). Linear regression analysis of Cued Platform Phase performance indicated that the slopes from the Non-Tg group at both 3 ($p = 0.0107$) and 9 months ($p = 0.0159$) are significantly different from zero, while the slopes of the m3R tau-Tg group at 3 ($p = 0.0802$) and 9 months ($p = 0.4330$) were not significantly different (Table 1). By the end of the third day on the Cued Platform Phase, m3R tau-Tg mice travelled significantly longer distances to locate the platform compared to their Non-Tg counterparts (Fig. 6a–b). These data suggest that the m3R tau-Tg mice are impaired in identifying visual cues. In the Hidden Platform Phase, m3R tau-Tg mice at both 3 and 9 months travelled significantly longer to the platform compared to Non-Tg mice (Fig. 6a–b). No significant differences in beam breaks were detected between m3R tau-Tg and Non-Tg in the spontaneous locomotor activity test at either age, implying general motor function is intact (Fig. 6c). Two way ANOVA analysis determined a significant main effect in genotype ($F_{(1,81)} = 27.42$, $p < 0.0001$) but not age ($F_{(1,43)} = 18.83$, $p < 0.0001$) as well as a significant genotype × age interaction ($F_{(1,81)} = 4.911$, $p < 0.0295$). Bonferroni post-hoc analysis determined that entries into the platform zone were significantly less in 9 month old m3R tau-Tg mice in the probe trial, suggesting m3R tau-Tg mice cannot retain spatial cues with age (Fig. 6d). Analysis through Two way ANOVA also found a significant main effect in age ($F_{(1,81)} = 10.22$, $p < 0.0001$) and genotype ($F_{(1,81)} = 32.34$, $p = 0.0020$) as well as a significant genotype x age interaction ($F_{(1,81)} = 5.651$, $p < 0.0198$) in the visible probe test. 9 month old m3R tau-Tg mice spent significantly more time locating the visible platform compared to Non-Tg, as determined by post hoc analysis (Fig. 6e). No significant difference was detected between sexes in the visible probe test (Supplementary Fig. S3). Together, these data suggest that m3R tau-Tg mice perform poorly in the MWM due to the inability to quickly locate a visible platform.

4. Discussion

Our study contributes to understanding retinal tau pathophysiology by conducting an in-depth assessment of the impact of mutant 3R tau in the retina, focusing on RGCs. Previous retinal studies in mouse models overexpressing mutant 4R tau demonstrated retinal dysfunction or degeneration (Gasparini et al., 2011; Harrison et al., 2019; Ho et al., 2015; Mazzaro et al., 2016), while mouse models expressing human tau failed to exhibit any retinopathy (Rodriguez et al., 2018), bringing into question how tau may mediate retinal pathology. In our present study, we show that expression of aggregate mutant 3R tau, which coincided with upregulation of caspase-2 throughout the retina, induced region-specific reduction in RGC cell density and visual impairment.

When using mouse models, it is important that the phenotype bears relevance to the biology of human disease. Transgene expression in the m3R tau-Tg and P301S mouse lines is driven by the promoter of Thy-1, a gene expressed in 60% of RGCs and 90% of displaced ACs (Raymond et al., 2008; Schmid et al., 1995). Our immunohistochemical analysis confirms expression of mutant 3R tau and hyperphosphorylated tau is restricted to the IPL and GCL (Fig. 1, Fig. 2), in line with the P301S mouse line expressing mutant 4R tau (Gasparini et al., 2011). Selective expression of mutant tau driven by the Thy-1 promoter may bias our study and not capture the entirety of tau retinopathy. However,

elevated levels of phosphorylated tau are observed in both the GCL and IPL in models of retinopathy, (Chiasseu et al., 2016; Zhu et al., 2018) as well as in the horizontal cells and IPL of glaucoma cases, (Gupta et al., 2008), highlighting the relevance of pathologic tau in RGC-related degeneration. Interestingly, 3R tau expression is not homogenous throughout the inner retina (Fig. 1), despite previous results of the Thy-1-mediated fluorescent protein expression evenly throughout the GCL (Raymond et al., 2008). It is possible that this observation is related to unknown interactions with transgene expression and an artefact of the system. However, hyperphosphorylated tau in post-mortem retinal tissue from AD cases was prominent in the retinal periphery (den Haan et al., 2018). Distribution of RGCs is heterogenous throughout the retina, segregated topologically to capture specific aspects of the visual field (Bleckert et al., 2014). Topological assessment of RGCs in the dorsal versus ventral region of the m3R tau-Tg retina would provide more insight into the region-specific expression of 3R tau. Our regional assessment of RBPMS expression suggests that region-specific selectivity of RGCs may occur in the m3R tau-Tg retina (Fig. 3e–f). Additionally, we observed caspase-2 upregulation in 3R tau-positive cells of the m3R tau-Tg retina (Fig. 5), which further implicates the peripheral region as a susceptible region in protein aggregate diseases (Koronyo et al., 2017).

To probe deeper into the mechanisms of mutant 3R tau retinal pathology, we implemented an unbiased generalized assessment of the 3R tau-Tg retina transcriptome, which identified pathways known to be involved in tau-mediated neuropathy. Pathways implicated in inflammation and cell death were enriched in our samples (Fig. 4). Retinal thinning and loss of RGCs are observed in the retinas of mice overexpressing human mutant tau PS301L (Harrison et al., 2019; Ho et al., 2015) but not P301S mice (Gasparini et al., 2011). While this may suggest a difference in severity between the mutations, the retinal studies done with the P301S line used young mice, only as old as 5 months. A reduction of RGC axon density was observed with increased aggregated tau in 5 month old P301S mice. Formation of fibrillary tau deposits in the retina increased with age in mice overexpressing the human mutant tau P301S, with the number of deposits peaking at 6.5 months (Schön et al., 2012). These data suggest that tau aggregation may impact RGC axons in early tauopathy and lead to the upregulation of cell death components such as caspase-2 in later stages of tauopathy after the peak of fibrillary formation. Mouse models harboring mutant variants of tau specific to human neurodegenerative disorders exhibit retinal disruption, suggesting that the mutation rather than the imbalance of tau isoforms mediates retinal pathogenesis.

Mitochondrial dysfunction is common in neurodegenerative diseases, including those mediated by tau (Kawamata and Manfredi, 2017; Lin and Beal, 2006; Pérez et al., 2018). Our dataset corroborates previous studies that characterized the downregulation of multiple subunits in mitochondrial respiratory Complex I (NADH: ubiquinone oxidoreductase) (Fig. 4b). In line with our molecular observations, irregular mitochondria, an indication of mitochondrial distress, were reported in m3R tau-tg brains (Rockenstein et al., 2015). Enzymatic activity of Complex I was uniquely decreased in the brains of transgenic mouse lines overexpressing tau (David et al., 2005; Rhein et al., 2009). Furthermore, transcript reduction of Complex I subunit Ndufa1 in the eye resulted in retinal thinning and RGC loss (Qi et al., 2003). In summary, these data suggest mutant 3R tau overexpression leads to the

specific reduction of essential Complex I subunit genes, possibly contributing to the retinal thinning observed in m3R tau-Tg mice.

Degeneration of RGCs is mediated by the cysteine aspartate proteases known as caspases in development, traumatic injury and retinal degenerative events (Thomas et al., 2017). Caspases are known for their role in the apoptosis pathway, with caspase-2 implicated in stress-induced apoptosis, including cytoskeleton disruption (Ho et al., 2008; Janssens and Tinel, 2012; Lassus et al., 2002). In the retina, photoreceptor cell death is mediated by caspase-9 while caspase-2 is implicated in RGC degeneration (Thomas et al., 2018). Like 3R tau, caspase-2 is highly expressed in the murine brain and retina during development and downregulated in adulthood (Kojima et al., 1998; Kumar et al., 1992). Multiple caspases are upregulated in retina during injury and disease, but downregulation of caspase-2 transcript through RNA interference and pharmacological inhibition proved to be sufficient for RGC survival (Ahmed et al., 2011; Vigneswara et al., 2012). Activated caspase-2 is also upregulated in models of glaucoma and optic neuritis, further suggesting that caspase-2 initiates RGC degeneration (Lidster et al., 2013; Reinehr et al., 2020). Processing of tau by caspase-2 leads to impairment of cognitive and synaptic function in a model of Huntington's disease (Zhao et al., 2016). While increased caspase-2 expression was seen in m3R tau-Tg retinas, it is unclear how caspase-2 and tau may interact. Further analysis into caspase-2 expression and function would elucidate the relationship between mutant 3R tau and caspase-2 in tau mediated cell death. Experiments using pharmacological inhibition or RNA interference would be ideal to further assess caspase-2 role in m3Rtau-Tg retinas.

There are several limitations in our study. While transcriptomic analysis of m3R tau-Tg retinas highlighted pathways supported by existing literature and provided tremendous insight (Fig. 4), the high variability within samples limited the breadth of our analysis. MDS analysis showed that there was high variance in gene expression within the 3 month group regardless of phenotype, while overall gene expression among the 9 month group was consistent. Immunohistochemical analysis of 3 month mice established stable 3R tau expression in m3R tau-Tg mice (Fig. 1). Retinal neurons reach the correct laminar layer and adult morphologies by 2 weeks of age (Reese, 2011), but other environmental variables may influence the retinal transcriptome. Therefore, an increase in sample size is necessary to mitigate sources of variation. A recent study implementing RNA-seq analysis of retinas from transgenic mice overexpressing amyloid precursor protein (APP) and Presenilin 1 (PSEN1) observed activation of pathways such as the JAK/STAT pathway (Chintapaludi et al., 2020). However, differential gene expression occurred prior to plaque formation, leading the authors to conclude that the observed changes were artificially driven by the overexpression of mutant APP and PSEN1. While we acknowledge that artificial results may arise when using transgenic mice, our study focused on the effects of mutant 3R tau isoform imbalance, a known mechanism of tauopathy, specifically in the retina.

In accordance with previous studies, m3R tau-Tg mice spent more time completing the MWM compared to Non-Tg mice and did not improve in locating the platform in the Cued Platform Phase (Fig. 6a–b, Table 1) (Arner et al., 2018; Rockenstein et al., 2015; Spencer et al., 2018). Other mouse strains of retinal degeneration exhibited similar latency times in the Cued Platform Phase of the MWM, further implying the poor performance of the m3R

tau-Tg mice may be due to retinal impairment (Brown and Wong, 2007). Visual processing is a multi-organ process, and other brain regions responsible for processing retinal stimuli may factor into visual loss seen in m3R tau-Tg mice. Our study focuses on the retina, the organ that processes visual light to neural signal. Future studies will look into the role of the other regions such as the thalamus and cortex, two regions shown to express high levels of 3R tau. In addition, future tests assessing the functionality of the m3R tau-Tg retina would provide further evidence that retinal 3R tau expression impairs the retina. However, while the test does test overall activity, the majority of the data derived from ERG is from photoreceptor activity, a cell type that we did not see any tau pathology. Taken together, retinal degeneration may factor into overall behavioral results, and experimental designs should consider measurements of visual detection to account for visual impairment.

5. Conclusion

In summary, our data indicate shifting tau isoform expression by overexpressing pathological 3R tau renders RGCs susceptible to neurodegeneration through altering multiple neurodegenerative pathways. Future studies using inhibitors of caspase-2 and kinases associated with tau modification to dissect the relationship between caspase-2 and 3R tau would greatly illuminate the underlying mechanisms driving RGC degeneration. Equipment to measure retinal health and activity in a non-invasive, in vivo manner would provide much needed temporal and functional data. Furthermore, our findings, in combination with current technology, highlight the value of the m3R tau-Tg mouse line in therapeutic development.

Supplementary Material

Refer to Web version on PubMed Central for supplementary material.

Acknowledgements

This work was supported by Awards AG018440, AG062429 and AG070595 to R.A.R and from the National Institute on Aging, USA.

References

Ahmed Z, Kalinski H, Berry M, Almasieh M, Ashush H, Slager N, Brafman A, Spivak I, Prasad N, Mett I, Shalom E, Alpert E, Di Polo A, Feinstein E, Logan A, 2011. Ocular neuroprotection by siRNA targeting caspase-2. Cell Death Dis. 2, e173. 10.1038/cddis.2011.54. [PubMed: 21677688]

Arendt T, Stieler JT, Holzer M, 2016. Tau and tauopathies. Brain Res. Bull. 126, 238–292. 10.1016/j.brainresbull.2016.08.018. [PubMed: 27615390]

Arner A, Rockenstein E, Mante M, Florio J, Masliah D, Salehi B, Adame A, Overk C, Masliah E, Rissman RA, 2018. Increased vulnerability of the hippocampus in transgenic mice overexpressing APP and triple repeat tau. J. Alzheimers Dis. 61, 1201–1219. 10.3233/JAD-170388. [PubMed: 29332037]

Bleckert A, Schwartz GW, Turner MH, Rieke F, Wong ROL, 2014. Visual space is represented by nonmatching topographies of distinct mouse retinal ganglion cell types. Curr. Biol. 24, 310–315. 10.1016/j.cub.2013.12.020. [PubMed: 24440397]

Brown RE, Wong AA, 2007. The influence of visual ability on learning and memory performance in 13 strains of mice. Learn. Mem. 14, 134–144. 10.1101/lm.473907. [PubMed: 17351136]

Chiasseu M, Cueva Vargas JL, Destroismaisons L, Vande Velde C, Leclerc N, Di Polo A, 2016. Tau accumulation, altered phosphorylation, and missorting promote neurodegeneration in glaucoma. J. Neurosci. 36, 5785. 10.1523/JNEUROSCI.3986-15.2016. [PubMed: 27225768]

Chintapaludi SR, Uyar A, Jackson HM, Acklin CJ, Wang X, Sasner M, Carter GW, Howell GR, 2020. Staging Alzheimer's Disease in the Brain and Retina of B6.APP/PS1 mice by transcriptional profiling. J. Alzheimers Dis. 73, 1421–1434. 10.3233/JAD-190793. [PubMed: 31929156]

David DC, Hauptmann S, Scherping I, Schuessel K, Keil U, Rizzu P, Ravid R, Dröse S, Brandt U, Müller WE, Eckert A, Götz J, 2005. Proteomic and functional analyses reveal a mitochondrial dysfunction in P301L tau transgenic mice. J. Biol. Chem. 280, 23802–23814. 10.1074/jbc.M500356200. [PubMed: 15831501]

Diamond JS, 2017. Inhibitory interneurons in the retina: types, circuitry, and function. Annu. Rev. Vis. Sci. 3, 1–24. 10.1146/annurev-vision-102016-061345. [PubMed: 28617659]

Fritsche LG, Fariss RN, Stambolian D, Abecasis GR, Curcio CA, Swaroop A, 2014. Age-related macular degeneration: genetics and biology coming together. Annu. Rev. Genomics Hum. Genet. 15, 151–171. 10.1146/annurev-genom-090413-025610. [PubMed: 24773320]

Gasparini L, Anthony Crowther R, Martin KR, Berg N, Coleman M, Goedert M, Spillantini MG, 2011. Tau inclusions in retinal ganglion cells of human P301S tau transgenic mice: effects on axonal viability. Neurobiol. Aging32, 419–433. 10.1016/j.neurobiolaging.2009.03.002. [PubMed: 19356824]

Goedert M, Spillantini MG, Jakes R, Rutherford D, Crowther RA, 1989. Multiple isoforms of human microtubule-associated protein tau: sequences and localization in neurofibrillary tangles of Alzheimer's disease. Neuron3, 519–526. 10.1016/0896-6273(89)90210-9. [PubMed: 2484340]

Goedert M, Falcon B, Zhang W, Ghetti B, Scheres SHW, 2018. Distinct conformers of assembled tau in Alzheimer's and Pick's diseases. Cold Spring Harb. Symp. Quant. Biol. 83, 163–171. 10.1101/sqb.2018.83.037580. [PubMed: 30886056]

Gupta N, Fong J, Ang LC, Yücel YH, 2008. Retinal tau pathology in human glaucomas. Can. J. Ophthalmol. 43, 53–60. 10.3129/i07-185. [PubMed: 18219347]

den Haan J, Morrema THJ, Verbraak FD, de Boer JF, Scheltens P, Rozemuller AJ, Bergen AAB, Bouwman FH, Hoozemans JJ, 2018. Amyloid-beta and phosphorylated tau in post-mortem Alzheimer's disease retinas. Acta Neuropathol. Commun. 610.1186/s40478-018-0650-x. [PubMed: 29378654]

Harrison IF, Whitaker R, Bertelli PM, O'Callaghan JM, Csincsik L, Bocchetta M, Ma D, Fisher A, Ahmed Z, Murray TK, O'Neill MJ, Rohrer JD, Lythgoe MF, Lengyel I, 2019. Optic nerve thinning and neurosensory retinal degeneration in the rTg4510 mouse model of frontotemporal dementia. Acta Neuropathol. Commun. 7, 4. 10.1186/s40478-018-0654-6. [PubMed: 30616676]

Ho LH, Read SH, Dorstyn L, Lambrusco L, Kumar S, 2008. Caspase-2 is required for cell death induced by cytoskeletal disruption. Oncogene27, 3393–3404. 10.1038/sj.onc.1211005. [PubMed: 18193089]

Ho WL, Leung Y, Cheng SSY, Lok CKM, Ho Y-S, Baum L, Yang X, Chiu K, Chang RC-C, 2015. Investigating degeneration of the retina in young and aged tau P301L mice. Life Sci. 124, 16–23. 10.1016/j.lfs.2014.12.019. [PubMed: 25592136]

Hogg M, Grujic ZM, Baker M, Demirci S, Guillozet AL, Sweet AP, Herzog LL, Weintraub S, Mesulam M-M, LaPointe NE, Gamblin TC, Berry RW, Binder LI, de Silva R, Lees A, Espinoza M, Davies P, Grover A, Sahara N, Ishizawa T, Dickson D, Yen S-H, Hutton M, Bigio EH, 2003. The L266V tau mutation is associated with frontotemporal dementia and Pick-like 3R and 4R tauopathy. Acta Neuropathol. 106, 323–336. 10.1007/s00401-003-0734-x. [PubMed: 12883828]

Hoon M, Okawa H, Della Santina L, Wong ROL, 2014. Functional architecture of the retina: development and disease. Prog. Retin. Eye Res. 42, 44–84. 10.1016/j.preteyeres.2014.06.003. [PubMed: 24984227]

Janssens S, Tinel A, 2012. The PIDDosome, DNA-damage-induced apoptosis and beyond. Cell Death Differ. 19, 13–20. 10.1038/cdd.2011.162. [PubMed: 22095286]

Josephs KA, 2017. Current understanding of neurodegenerative diseases associated with the protein tau. Mayo Clin. Proc. 92, 1291–1303. 10.1016/j.mayocp.2017.04.016. [PubMed: 28778262]

Kawamata H, Manfredi G, 2017. Proteinopathies and OXPHOS dysfunction in neurodegenerative diseases. J. Cell Biol. 216, 3917–3929. 10.1083/jcb.201709172. [PubMed: 29167179]

Kojima M, Asahi M, Kikuchi H, Hashimoto N, Noda M, Hoshimaru M, 1998. Expression of Nedd2/ICH-1 (caspase-2) in the developing rat retina. Neurosci. Res. 31, 211–217. 10.1016/S0168-0102(98)00039-X. [PubMed: 9809666]

Koronyo Y, Biggs D, Barron E, Boyer DS, Pearlman JA, Au WJ, Kile SJ, Blanco A, Fuchs D-T, Ashfaq A, Frautschy S, Cole GM, Miller CA, Hinton DR, Verdooner SR, Black KL, Koronyo-Hamaoui M, 2017. Retinal amyloid pathology and proof-of-concept imaging trial in Alzheimer's disease. JCI Insight2. 10.1172/jci.insight.93621.

Kovacs GG, 2015. Invited review: neuropathology of tauopathies: principles and practice. Neuropathol. Appl. Neurobiol. 41, 3–23. 10.1111/nan.12208. [PubMed: 25495175]

Kumar S, Tomooka Y, Noda M, 1992. Identification of a set of genes with developmentally down-regulated expression in the mouse brain. Biochem. Biophys. Res. Commun. 185, 1155–1161. 10.1016/0006-291X(92)91747-E. [PubMed: 1378265]

Lassus P, Opitz-Araya X, Lazebnik Y, 2002. Requirement for Caspase-2 in stress-induced apoptosis before mitochondrial Permeabilization. Science297, 1352. 10.1126/science.1074721. [PubMed: 12193789]

Law CW, Chen Y, Shi W, Smyth GK, 2014. Voom: precision weights unlock linear model analysis tools for RNA-seq read counts. Genome Biol. 15, R29. 10.1186/gb-2014-15-2-r29. [PubMed: 24485249]

Lidster K, Jackson SJ, Ahmed Z, Munro P, Coffey P, Giovannoni G, Baker MD, Baker D, 2013. Neuroprotection in a novel mouse model of multiple sclerosis. PLoS One8, e79188. 10.1371/journal.pone.0079188. [PubMed: 24223903]

Lin MT, Beal MF, 2006. Mitochondrial dysfunction and oxidative stress in neurodegenerative diseases. Nature443, nature05292. 10.1038/nature05292.

Mancarci BO, Toker L, Tripathy SJ, Li B, Rocco B, Sibille E, Pavlidis P, 2017. Cross-laboratory analysis of brain cell type Transcriptomes with applications to interpretation of bulk tissue data. eNeuro4. 10.1523/ENEURO.0212-17.2017 (ENEURO.0212–17.2017).

Masland RH, 2012. The neuronal organization of the retina. Neuron76, 266–280. 10.1016/j.neuron.2012.10.002. [PubMed: 23083731]

Mazzaro N, Barini E, Spillantini MG, Goedert M, Medini P, Gasparini L, 2016. Tau-driven neuronal and neurotrophic dysfunction in a mouse model of early tauopathy. J. Neurosci. 36, 2086. 10.1523/JNEUROSCI.0774-15.2016. [PubMed: 26888921]

Menon M, Mohammadi S, Davila-Velderrain J, Goods BA, Cadwell TD, Xing Y, Stemmer-Rachamimov A, Shalek AK, Love JC, Kellis M, Hafler BP, 2019. Single-cell transcriptomic atlas of the human retina identifies cell types associated with age-related macular degeneration. Nat. Commun. 10, 4902. 10.1038/s41467-019-12780-8. [PubMed: 31653841]

Patro R, Duggal G, Love MI, Irizarry RA, Kingsford C, 2017. Salmon provides fast and bias-aware quantification of transcript expression. Nat. Methods14, 417–419. 10.1038/nmeth.4197. [PubMed: 28263959]

Pérez MJ, Jara C, Quintanilla RA, 2018. Contribution of tau pathology to mitochondrial impairment in neurodegeneration. Front. Neurosci. 12, 441. 10.3389/fnins.2018.00441. [PubMed: 30026680]

Qi X, Lewin AS, Hauswirth WW, Guy J, 2003. Suppression of complex I gene expression induces optic neuropathy. Ann. Neurol. 53, 198–205. 10.1002/ana.10426. [PubMed: 12557286]

Raymond ID, Vila A, Huynh U-CN, Brecha NC, 2008. Cyan fluorescent protein expression in ganglion and amacrine cells in a thy1-CFP transgenic mouse retina. Mol. Vis. 14, 1559–1574. [PubMed: 18728756]

Reese BE, 2011. Development of the retina and optic pathway. Vis. Res. 51, 613–632. 10.1016/j.visres.2010.07.010. [PubMed: 20647017]

Reinehr S, Buschhorn V, Mueller-Buehl AM, Goldmann T, Grus FH, Wolfrum U, Dick HB, Joachim SC, 2020. Occurrence of retinal ganglion cell loss via autophagy and apoptotic pathways in an autoimmune glaucoma model. Curr. Eye Res. 1–12. 10.1080/02713683.2020.1716987.

Rhein V, Song X, Wiesner A, Ittner LM, Baysang G, Meier F, Ozmen L, Bluethmann H, Dröse S, Brandt U, Savaskan E, Czech C, Götz J, Eckert A, 2009. Amyloid-β and tau synergistically impair

the oxidative phosphorylation system in triple transgenic Alzheimer's disease mice. Proc. Natl. Acad. Sci. U. S. A. 106, 20057. 10.1073/pnas.0905529106. [PubMed: 19897719]

Rissman RA, Poon WW, Blurton-Jones M, Oddo S, Torp R, Vitek MP, LaFerla FM, Rohn TT, Cotman CW, 2004. Caspase-cleavage of tau is an early event in Alzheimer disease tangle pathology. J. Clin. Invest. 114, 121–130. 10.1172/JCI20640. [PubMed: 15232619]

Ritchie ME, Phipson B, Wu D, Hu Y, Law CW, Shi W, Smyth GK, 2015. Limma powers differential expression analyses for RNA-sequencing and microarray studies. Nucleic Acids Res. 43, e47. 10.1093/nar/gkv007. [PubMed: 25605792]

Robinson MD, Oshlack A, 2010. A scaling normalization method for differential expression analysis of RNA-seq data. Genome Biol. 11, R25. 10.1186/gb-2010-11-3-r25. [PubMed: 20196867]

Rockenstein E, Overk CR, Ubhi K, Mante M, Patrick C, Adame A, Bisquert A, Trejo-Morales M, Spencer B, Masliah E, 2015. A novel triple repeat mutant tau transgenic model that mimics aspects of Pick's Disease and fronto-temporal tauopathies. PLoS One10, e0121570. 10.1371/journal.pone.0121570. [PubMed: 25803611]

Rodriguez L, Mdzomba JB, Joly S, Boudreau-Laprise M, Planel E, Pernet V, 2018. Human tau expression does not induce mouse retina neurodegeneration, suggesting differential toxicity of tau in brain vs. retinal neurons. Front. Mol. Neurosci. 11, 293. 10.3389/fnmol.2018.00293. [PubMed: 30197586]

Schmid S, Guenther E, Kohler K, 1995. Changes in Thy-1 antigen immunoreactivity in the rat retina during pre- and postnatal development. Neurosci. Lett. 199, 91–94. 10.1016/0304-3940(95)12020-5. [PubMed: 8584251]

Schön C, Hoffmann NA, Ochs SM, Burgold S, Filser S, Steinbach S, Seeliger MW, Arzberger T, Goedert M, Kretzschmar HA, Schmidt B, Herms J, 2012. Long-term in vivo imaging of fibrillar tau in the retina of P301S transgenic mice. PLoS One7, e53547. 10.1371/journal.pone.0053547. [PubMed: 23300938]

Siegert S, Cabuy E, Scherf BG, Kohler H, Panda S, Le Y-Z, Fehling HJ, Gaidatzis D, Stadler MB, Roska B, 2012. Transcriptional code and disease map for adult retinal cell types. Nat. Neurosci. 15, 487–495. 10.1038/nn.3032. [PubMed: 22267162]

Soneson C, Love MI, Robinson MD, 2015. Differential analyses for RNA-seq: transcript-level estimates improve gene-level inferences. F1000Res4, 1521–1521. 10.12688/f1000research.7563.2. [PubMed: 26925227]

Spencer B, Brüschweiler S, Sealey-Cardona M, Rockenstein E, Adame A, Florio J, Mante M, Trinh I, Rissman RA, Konrat R, Masliah E, 2018. Selective targeting of 3 repeat Tau with brain penetrating single chain antibodies for the treatment of neurodegenerative disorders. Acta Neuropathol. 136, 69–87. 10.1007/s00401-018-1869-0. [PubMed: 29934874]

Subramanian A, Tamayo P, Mootha VK, Mukherjee S, Ebert BL, Gillette MA, Paulovich A, Pomeroy SL, Golub TR, Lander ES, Mesirov JP, 2005. Gene set enrichment analysis: a knowledge-based approach for interpreting genome-wide expression profiles. Proc. Natl. Acad. Sci. U. S. A. 102, 15545–15550. 10.1073/pnas.0506580102. [PubMed: 16199517]

Thomas CN, Berry M, Logan A, Blanch RJ, Ahmed Z, 2017. Caspases in retinal ganglion cell death and axon regeneration. Cell Death Dis. 3, 17032–17032. 10.1038/cddiscovery.2017.32.

Thomas CN, Thompson AM, McCance E, Berry M, Logan A, Blanch RJ, Ahmed Z, 2018. Caspase-2 mediates site-specific retinal ganglion cell death after blunt ocular injury. Invest. Ophthalmol. Vis. Sci. 59, 4453–4462. 10.1167/iovs.18-24045. [PubMed: 30193318]

Vigneswara V, Berry M, Logan A, Ahmed Z, 2012. Pharmacological inhibition of Caspase-2 protects Axotomised retinal ganglion cells from apoptosis in adult rats. PLoS One7, e53473. 10.1371/journal.pone.0053473. [PubMed: 23285297]

Voigt AP, Whitmore SS, Flamme-Wiese MJ, Riker MJ, Wiley LA, Tucker BA, Stone EM, Mullins RF, Scheetz TE, 2019. Molecular Characterization of foveal versus peripheral human retina by single-cell RNA sequencing. Exp. Eye Res. 184, 234–242. 10.1016/j.exer.2019.05.001. [PubMed: 31075224]

Vorhees CV, Williams MT, 2006. Morris water maze: procedures for assessing spatial and related forms of learning and memory. Nat. Protoc. 1, 848–858. 10.1038/nprot.2006.116. [PubMed: 17406317]

Wang Y, Mandelkow E, 2016. Tau in physiology and pathology. Nat. Rev. Neurosci. 17, 22–35. 10.1038/nrn.2015.1. [PubMed: 26656254]

Yu G, Wang L-G, Han Y, He Q-Y, 2012. clusterProfiler: an R package for comparing biological themes among gene clusters. OMICS16, 284–287. 10.1089/omi.2011.0118. [PubMed: 22455463]

Zhao X, Kotilinek LA, Smith B, Hlynialuk C, Zahs K, Ramsden M, Cleary J, Ashe KH, 2016. Caspase-2 cleavage of tau reversibly impairs memory. Nat. Med. 22, 1268–1276. 10.1038/nm.4199. [PubMed: 27723722]

Zhu H, Zhang W, Zhao Y, Shu X, Wang W, Wang D, Yang Y, He Z, Wang X, Ying Y, 2018. GSK3β-mediated tau hyperphosphorylation triggers diabetic retinal neurodegeneration by disrupting synaptic and mitochondrial functions. Mol. Neurodegener. 13, 62. 10.1186/s13024-018-0295-z. [PubMed: 30466464]

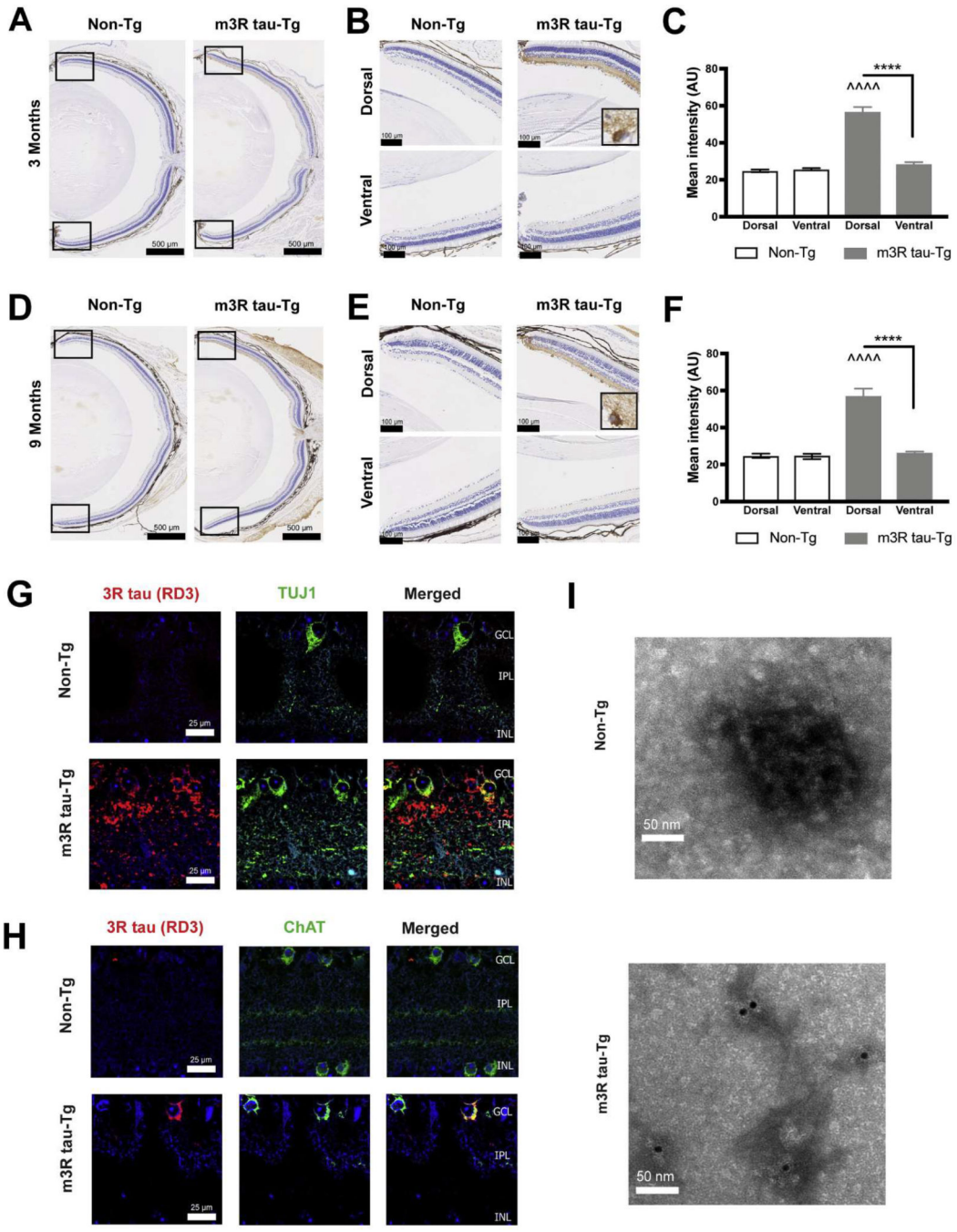

Fig. 1.

Region and cell-specific expression of 3R Tau in the murine retina. Representative micrographs of retinal cross-sections from a) 3 month Non-Tg and b) 3 month m3R tau-Tg immunostained for 3R tau and visualized with 3,3'-Diaminobenzidine (DAB). Highlighted regions depict the location of insets from the dorsal (top) and ventral (bottom) regions of the retina. c) Quantification of 3R tau immunostaining in the dorsal and ventral retina periphery of Non-tg mice (outlined white bars, $n = 6$) and m3R tau-Tg (grey bars, $n = 6$) at 3 months expressed as mean intensity (Arbitrary Units, AU). Measurements are represented as mean ±

standard error of the mean. d) 9 month Non-Tg and e) 9 month m3R tau-Tg immunostained for 3R tau and visualized with 3,3'-Diaminobenzidine (DAB). Highlighted regions depict the location of the dorsal (top) and ventral (bottom) regions of the retina. f) Quantification of 3R tau immunostaining in the dorsal and ventral retina periphery of Non-tg (outlined white bars, $n = 7$) and m3R tau-Tg (grey bars, $n = 4$) mice at 9 months expressed as mean intensity (AU). Measurements are represented as mean ± standard error of the mean. g) Representative images of cross sections from Non-Tg (top) and m3R tau-Tg retinas stained with RD3 (Red), an antibody specific to 3R tau and TUJ1 (green), a retinal ganglion cell marker. Scale bar is 25 μm. Total count of 3R tau positive stained cells along the GCL of h) 3 and i) 9 month retinal cross-sections. ^^^ $p < 0.0002$, ^^^^ $p < 0.0001$ m3R tau-Tg dorsal region compared to m3R tau-Tg ventral region. j) Representative images of cross sections from Non-Tg (top) and m3R tau-Tg retinas stained with 3R tau tg (Red) and choline acetyltransferase (ChAT) (green), a marker for cholinergic amacrine cells. Scale bar is 25 μm. **** $p < 0.0001$ m3R tau-Tg dorsal retina compared to Non-Tg dorsal and ventral. ^^^^ $p < 0.0001$ m3R tau-Tg dorsal retina compared to m3R tau-Tg ventral retina. GCL: ganglion cell layer, IPL: inner plexiform layer, INL: inner nuclear layer.

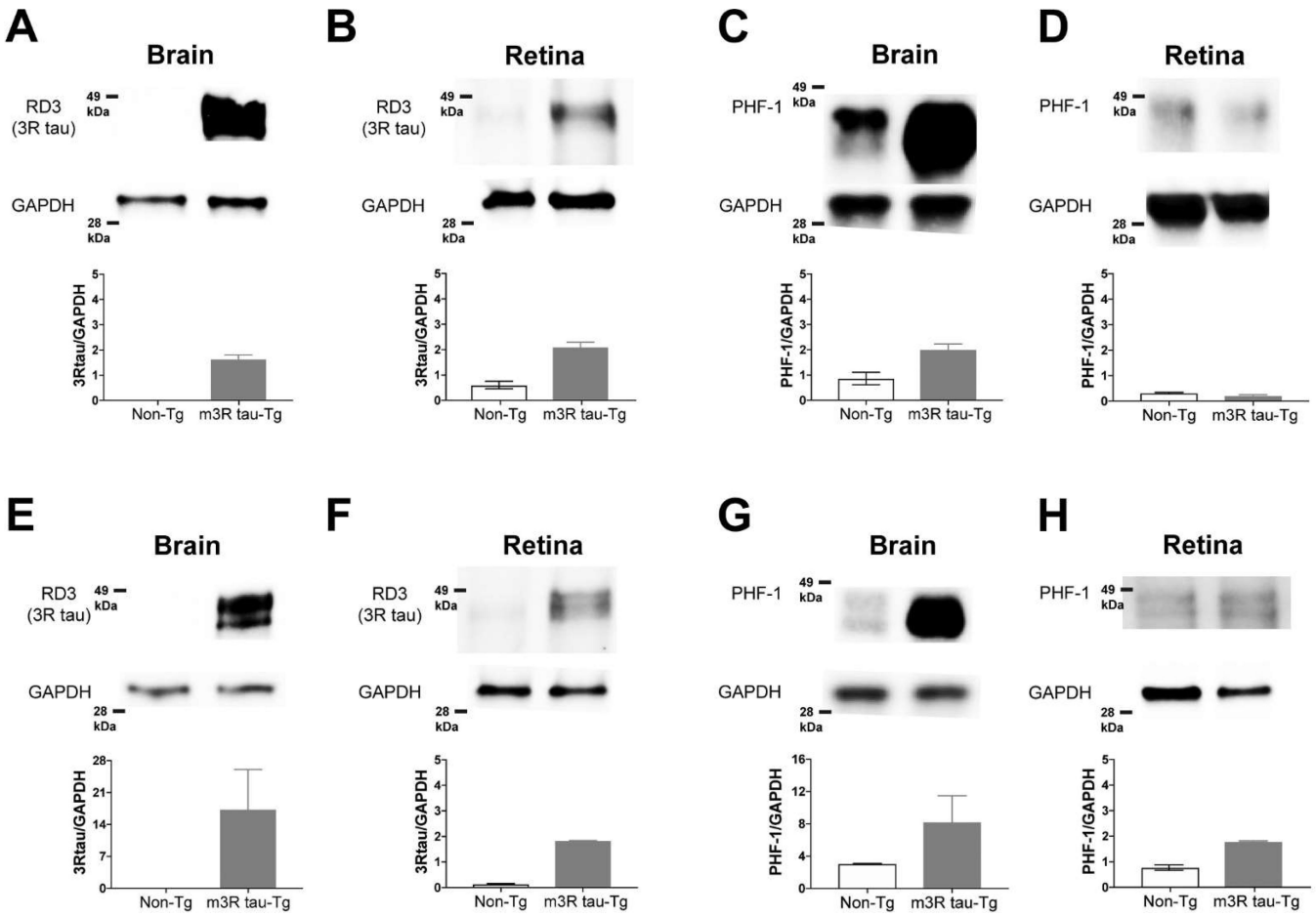

Fig. 2.

Hyperphosphorylation of 3R tau in the retina is restricted to the detergent insoluble fraction. Characterization of the 3R tau isoform in brain (a, c, e, g) and retina (b, d, f, h) from 9 month m3R tau-Tg and Non-Tg mice. Western blot analysis of brain and retina lysates the (a–d) RAB and (e–h) RIPA fraction. *Top:* Representative blot for (a–b, e–f) RD3, (c–d, g–h) PHF-1 and GAPDH. *Bottom:* Semi-quantitative measure of protein expression in Non-Tg (outlined white bars) and m3R tau-Tg tissues (grey bards). $N = 2$.

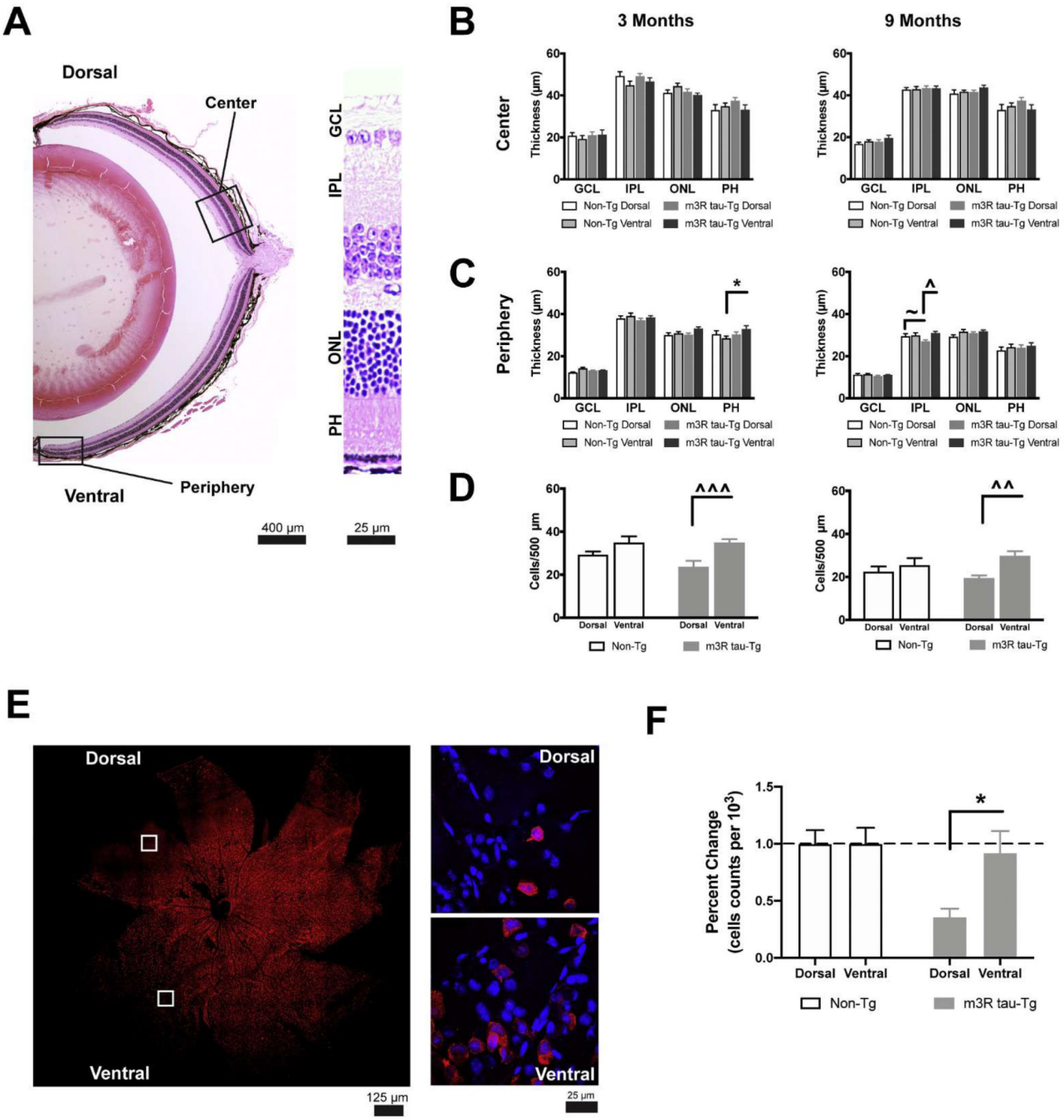

Fig. 3.

Expression of 3R tau alters the peripheral inner retina over time. a) Representative micrograph of a retinal cross-section illustrating orientation and regions measured. Center measurements were taken 500 µm from optic nerve and peripheral measurements were taken 500 µm from the edge. Right inset highlights the regions of measurement such the as ganglion cell layer (GCL), inner plexiform layer (IPL), outer nuclear layer (ONL) and photoreceptor layer (PH). Scale bar represents 400 µm in micrograph and 25 µm in inset. b) Center measurements of the GCL, IPL, ONL and PH of m3R tau-Tg and Non-Tg retinal

cross-sections at 3 months (Non-Tg $n = 10$, outlined bars; m3R tau-Tg, unlined grey bars, $n = 17$,) and 9 months (Non-Tg, outlined bars, $n = 9$; m3R tau-Tg, unlined grey bars, $n = 12$). Measurements were recorded in the dorsal (light shades) and ventral (dark shades) region of each retinal cross-section. c) Peripheral measurements of the GCL, IPL, ONL and PH layer of m3R tau-Tg and Non-Tg retinal cross-sections at 3 months (Non-Tg, outlined bars, $n = 10$; m3R tau-Tg, unlined grey bars, $n = 17$) and 9 months (Non-Tg, outlined bars, $n = 9$; m3R tau-Tg, unlined grey bars, $n = 12$). Measurements are represented as mean ± standard error of the mean. * $p < 0.0332$ m3R tau-Tg ventral region compared to Non-Tg ventral region. ^ $p < 0.0332$ m3R tau-Tg dorsal region compared to m3R tau-Tg ventral region. ~$p < 0.0254$ Non-Tg dorsal region compared to m3R tau-Tg dorsal region. d) Total count of hematoxylin stained cells along the GCL of retinal cross-sections at 3 months (Non-Tg, outlined white bars, $n = 9$; m3R tau-Tg, grey bars, $n = 9$;) and 9 months (Non-Tg, outlined white bars, $n = 9$; m3R tau-Tg, grey bars, $n = 9$). ^^ $p < 0.0021$, ^^^ $p < 0.0002$ m3R tau-Tg dorsal region compared to m3R tau-Tg ventral region. e) Composite image of a 9 month m3R tau-Tg retinal flatmount. Inset micrographs reflect the highlighted regions depicted on the flatmount. f) Quantification of RBPMS+ cells of retinal flatmounts at 9 months (Non-Tg, outlined white bars, $n = 4$; m3R tau-Tg, grey bars, $n = 4$). ~$p < 0.0384$ Non-Tg dorsal region compared to m3R tau-Tg dorsal region.

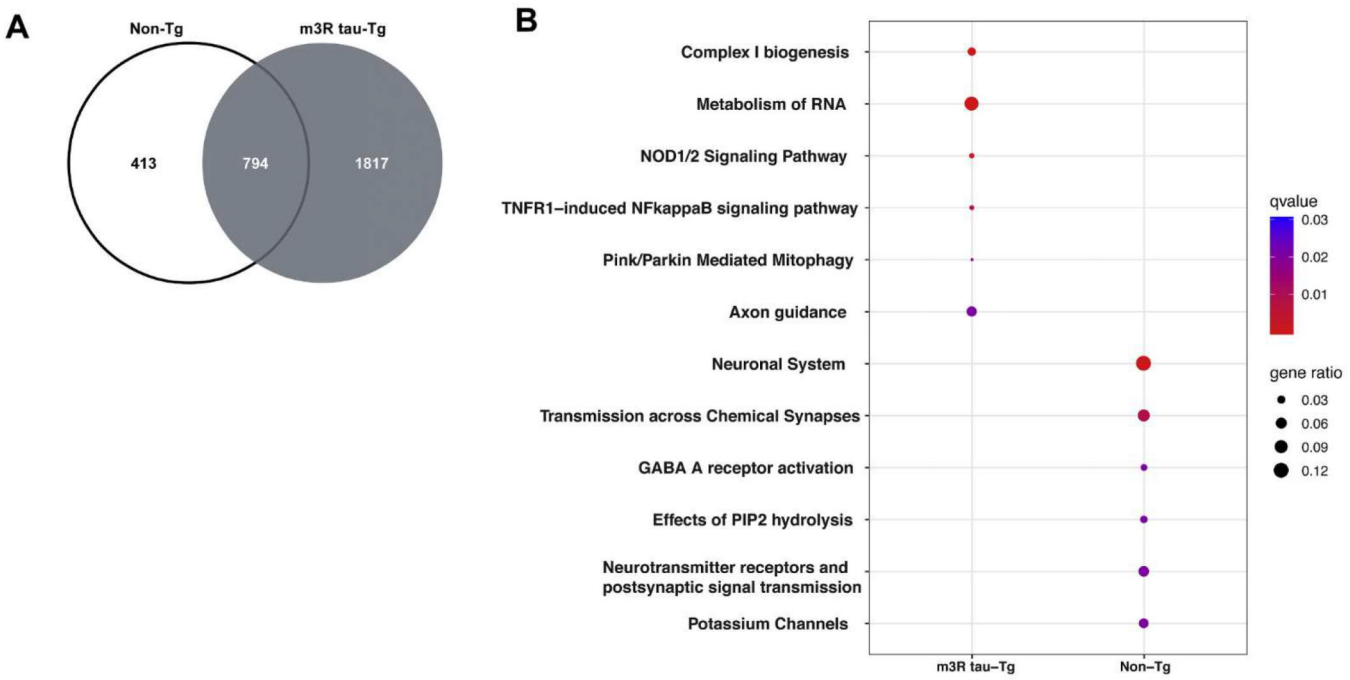

Fig. 4.

Transcriptional alterations due to 3R tau expression. a) Venn diagram of differentially expressed genes in Non-Tg (Outlined white region, $n = 4–5$) and m3R tau-Tg (Grey region, $n = 5$) retinas. Among the differentially expressed genes shared between genotypes, only two genes varied in expression direction. b) Top six biological pathways in which differentially expressed genes in m3R tau-Tg and Non-Tg clustered into. Circle size represents the gene ratio, and color depicts the qvalue of each biological pathway. Biological pathways are sourced from the REACTOME database.

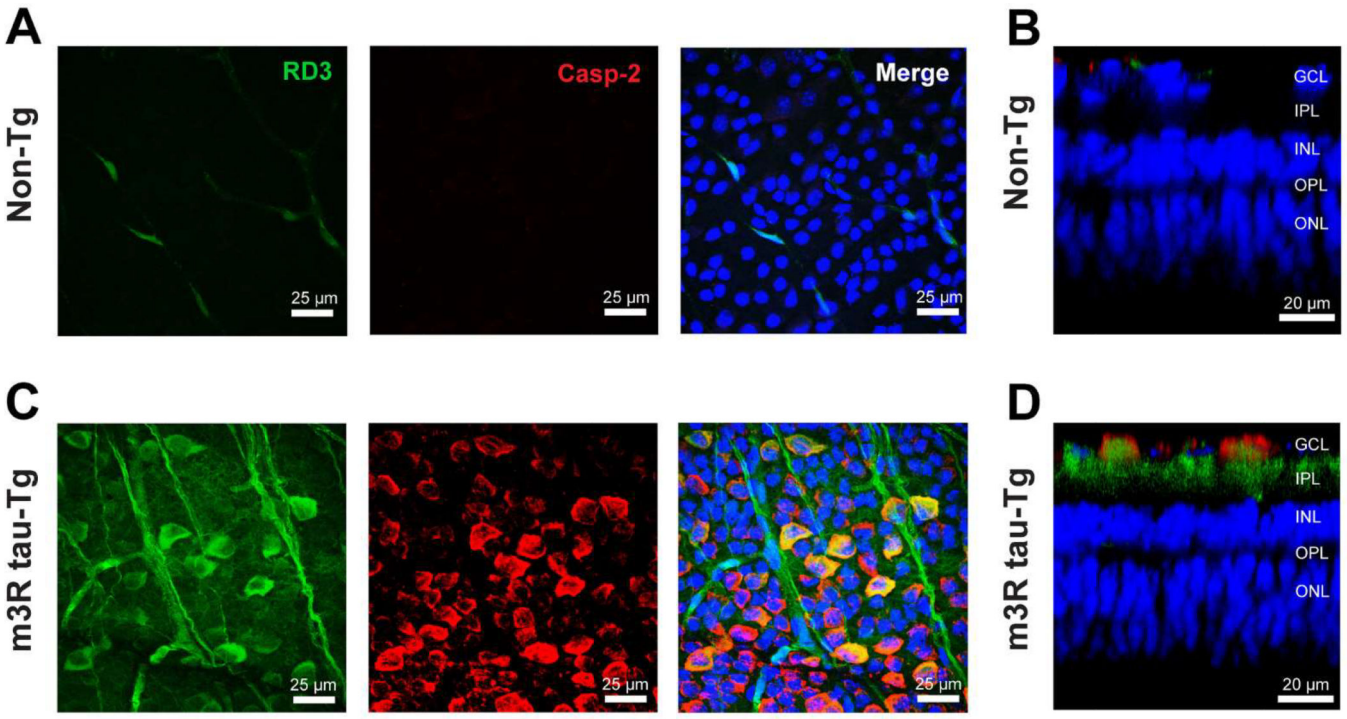

Fig. 5.

Increased expression of caspase-2 in 3R tau positive regions of the retina. Representative image of retinal tissue of retina from a) m3R tau-Tg and c) Non-Tg mouse, stained with 3R tau (green) and caspase-2 (red). Cross-section from a *Z*-stack of b) m3R tau-Tg and d) Non-Tg retinal tissue, indicating where the fluorescence signal lies in the retinal layers.

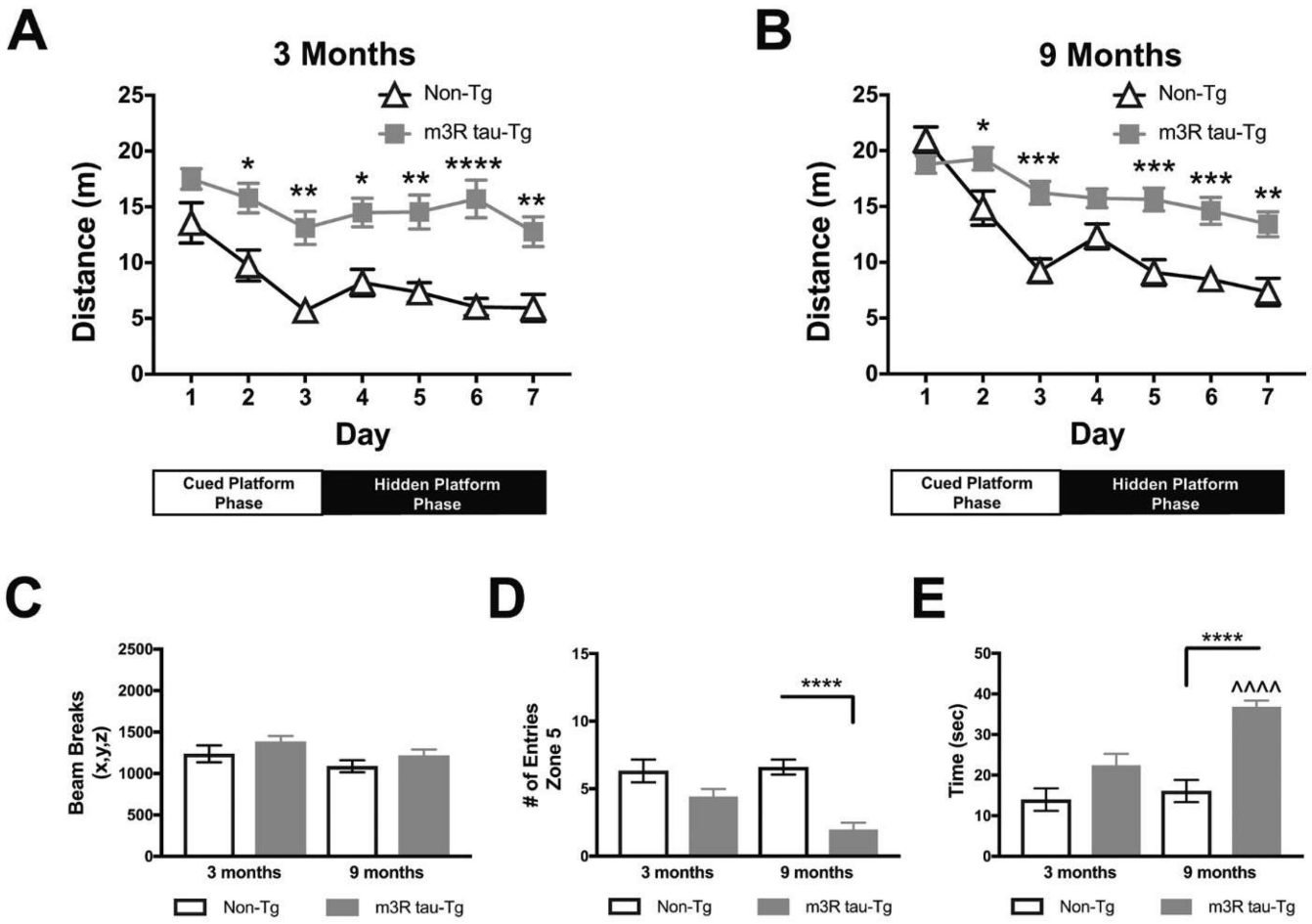

Fig. 6.

Mice over expressing mutant 3R tau exhibit visual as well as memory deficits in the Morris Water Maze. Performance of in the Morris Water Maze represented as Distance travelled (in meters) by Non-Tg (Outlined white triangles) and m3R tau-Tg (grey squares) mice at a) 3 months and b) 9 months. The Cued Platform Phase is conducted in the first three trials, where the platform is visible, while in the last four trials denote the hidden platform phase. c) Overall locomotor activity in Non-Tg (Outlined white bars) and m3R tau-Tg (Grey bars), measured in beam breaks along the x, y and z-axis. d) After completion of water maze testing, Non-Tg (Outlined white bars) and m3R tau-Tg (Grey bars) mice underwent the Probe trial to test for memory retention. e) Visual acuity was assessed in the Visual Probe by measuring time spent locating a visible platform in Non-Tg (Outlined white bars) and m3R tau-Tg (Grey bars). Mice used per genotype per age: m3R tau-Tg (3 month: $n = 17$, 9 month: $n = 12$), Non-Tg (3 month: $n = 10$, 9 month: $n = 9$). Measurements are represented as mean ± standard error of the mean. * $p < 0.0332$ m3R tau-Tg mice compared to Non-Tg mice, ** $p < 0.0021$ m3R tau-Tg mice compared to Non-Tg mice, *** $p < 0.0002$ m3R tau-Tg mice compared to Non-Tg mice, **** $p < 0.0001$ m3R tau-Tg mice compared to Non-Tg mice. ^^^^ $p < 0.0001$ 3 month m3R tau-Tg mice compared to 9 month m3R tau-Tg mice.

Table 1

Linear regression analysis of the Cued Platform Phase in the Morris Water Maze.

	Slope (Mean ± SEM)	R squared	F	*P* value
Non-Tg 3 months	−3.94 ± 0.06619	0.9997	3543	0.0107
Non-Tg 9 months	−5.879 ± 0.1472	0.9994	1594	0.0159
m3R tau-Tg 3 months	−2.202 ± 0.2789	0.9842	62.32	0.0802
m3R tau-Tg 9 months	−1.271 ± 1.028	0.6044	1.528	0.4330

Table 2

Clustering of differentially expressed genes by biological pathway from the m3R tau-Tg and Non-Tg retinal dataset.

Genotype	Pathway	Gene Ratio	p.adjust	qvalue	geneID
m3R tau-Tg	Complex I biogenesis	26/830	2.24E-10	1.92E-10	Ndufb7/Ndufb4/Ndufa3/Ndufa7/Ndufa8/Ndufa6/Ndufv3/Ndufa2/Ndufa1/Ndufa11/Ndufs5/Ndufb2/Ndufa13/Ndufb10/Ndufb9/Ndufb11/Ndufs6/Ndufb4c/ND4/ND6/Ndufb8/Ndufv2/Ndufc1/Ndufs3/Ndufc2/Ndufs7
m3R tau-Tg	Metabolism of RNA	68/830	0.00764056	0.00653788	Cnot6/Uba52/Ubc/Dhx15/Nxf1/Zmat5/Zc3h11a/Fau/Rps26/Ranbp2/Cnot6l/Psmb6/Rps25/Krr1/Rps28/Ddx6/Psmb2/Rps5/Ddx21/U2af1l4/Sf3b5/Srsf11/Sf3b6/Srsf1/Rnpc3/Snrpd2/Cpsf1/Rps21/Mtrex/Rbm5/Cdc5l/Psmc4/Papola/Ddx49/Exosc4/Tra2b/Rps9/Cnot1/Zfp473/Rps13/Rae1/Prpf4/Hbs1l/Hnrnpr/Cstf2/Thoc2/Psmd3/Utp6/Ddx46/Exosc5/Gpkow/Fyttd1/Lsm7/Polr2f/Srsf6/Srrm1/Sf3a2/Snrpf/Puf60/Casc3/Psmf1/Zcrb1/Upf3b/Snrpc/Las1l/Psmd4/Snrpd1/Polr2c
m3R tau-Tg	NOD1/2 Signaling Pathway	11/830	0.00471296	0.00403279	Uba52/Ubc/Tnfaip3/Itch/Map3k7/Casp2/Traf6/Mapk14/Tab2/Cyld/Chuk
m3R tau-Tg	TNFR1-induced NFkappaB signaling pathway	10/830	0.01108529	0.00948547	Uba52/Ubc/Tnfaip3/Map3k7/Otud7b/Xiap/Tab2/Cyld/Rack1/Chuk
m3R tau-Tg	Pink/Parkin Mediated Mitophagy	8/830	0.01032666	0.00883632	Uba52/Ubc/Sqstm1/Tomm40/Tomm7/Tomm20/Tomm6/Mfn1
m3R tau-Tg	Axon guidance	43/830	0.01943907	0.01663363	Tubb2a/Uba52/Creb1/Ubc/Tuba1a/Pdlim7/Tubb3/L1cam/Mapk8/Tubb2b/Vldlr/Pik3ca/Actg1/Arpc3/Hras/Rasa1/Mapk14/Gap43/Csnk2b/Rock2/Actb/Clta/Rap1gap/Pfn1/Map2k2/Dnm1/Col4a4/Ank3/Rhoc/Lypla2/Crmp1/Dpysl4/Akap5/Ncstn/Tln1/Plxnb1/Reln/Yes1/Col4a2/Psenen/Arhgap35/Ptpn11/Tuba4a
Non-Tg	Neuronal System	26/199	8.00E-06	7.92E-06	Grik3/Kcnh5/Gabrb2/Lin7a/Arhgef9/Homer2/Kcnk2/Gabra3/Kcna3/Rasgrf1/Kcnj8/Kcna2/Kcnj9/Gabra1/Aldh5a1/Flot1/Hcn2/Chat/Calm1/Kcnh1/Camk4/Epb41l1/Chrna7/Gng2/Gad2/Glrb
Non-Tg	Transmission across Chemical Synapses	17/199	0.00075863	0.00075038	Grik3/Gabrb2/Lin7a/Arhgef9/Gabra3/Rasgrf1/Kcnj9/Gabra1/Aldh5a1/Chat/Calm1/Camk4/Epb41l1/Chrna7/Gng2/Gad2/Glrb
Non-Tg	Neurotransmitter receptors and postsynaptic signal transmission	13/199	0.00250865	0.00248137	Grik3/Gabrb2/Arhgef9/Gabra3/Rasgrf1/Kcnj9/Gabra1/Calm1/Camk4/Epb41l1/Chrna7/Gng2/Glrb
Non-Tg	GABA A receptor activation	4/199	0.01847511	0.01827424	Gabrb2/Arhgef9/Gabra3/Gabra1
Non-Tg	Effects of PIP2 hydrolysis	5/199	0.01921635	0.01900742	Dgkg/Itpr1/Dgkz/Dgkh/Dgki
Non-Tg	Potassium Channels	9/199	0.02334709	0.02309324	Kcnh5/Kcnk2/Kcna3/Kcnj8/Kcna2/Kcnj9/Hcn2/Kcnh1/Gng2